

Thermodynamic magnetization of a strongly correlated two-dimensional electron system

S. V. Kravchenko,^{*} A. A. Shashkin,¹ S. Anissimova,
A. Venkatesan,² M. R. Sakr³

Physics Department, Northeastern University, Boston, Massachusetts 02115, USA

V. T. Dolgoplov

Institute of Solid State Physics, Chernogolovka, Moscow District 142432, Russia

T. M. Klapwijk

Kavli Institute of Nanoscience, Delft University of Technology, 2628 CJ Delft, The Netherlands

Abstract

We measure thermodynamic magnetization of a low-disordered, strongly correlated two-dimensional electron system in silicon. Pauli spin susceptibility is observed to grow critically at low electron densities — behavior that is characteristic of the existence of a phase transition. A new, parameter-free method is used to directly determine the spectrum characteristics (Landé g -factor and the cyclotron mass) when the Fermi level lies outside the spectral gaps and the inter-level interactions between quasiparticles are avoided. It turns out that, unlike in the Stoner scenario, the critical growth of the spin susceptibility originates from the dramatic enhancement of the effective mass, while the enhancement of the g -factor is weak and practically independent of the electron density.

Key words:

PACS: 71.30.+h, 73.40.Qv

^{*} Corresponding author

Email address: s.kravchenko@neu.edu (S. V. Kravchenko,).

¹ Permanent address: Institute of Solid State Physics, Chernogolovka, Moscow District 142432, Russia

² Present address: Department of Physics and Astronomy, University of British Columbia, Vancouver, BC V6T 1Z1, Canada

³ Present address: Department of Physics and Astronomy, UCLA, Los Angeles, CA 90095, USA

1 Introduction

Presently, theoretical description of interacting electron systems is restricted to two limiting cases: (i) weak electron-electron interactions (small ratio of the Coulomb and Fermi energies $r_s = E_C/E_F \ll 1$, high electron densities) and (ii) very strong electron-electron interactions ($r_s \gg 1$, very low electron densities). In the first case, conventional Fermi-liquid behavior [1] is established, while in the second case, formation of the Wigner crystal is expected [2] (for recent developments, see Ref. [3]). Numerous experiments performed in both three- (3D) and two-dimensional (2D) electron systems at intermediate interaction strengths ($1 \lesssim r_s \lesssim 5$) have not demonstrated any significant change in properties compared to the weakly-interacting regime (see, *e.g.*, Refs. [4,5]). It was not until recently that qualitative deviations from the weakly-interacting Fermi liquid behavior (in particular, the drastic increase of the effective electron mass with decreasing electron density) have been found in strongly correlated 2D electron systems ($r_s \gtrsim 10$) [6]. However, these findings have been based solely on the studies of a kinetic parameter (conductivity), which, in general, is not a characteristic of a state of matter.

The 2D electron system in silicon turns out to be a very convenient object for studies of the strongly correlated regime due to the large interaction strengths ($r_s > 10$ can be easily reached) and high homogeneity of the samples estimated (from the width of the magnetocapacitance minima in perpendicular magnetic fields) at about $4 \times 10^9 \text{ cm}^{-2}$ [7]. Here we report measurements of the thermodynamic magnetization and density of states in such a low-disordered, strongly correlated 2D electron system in silicon. We concentrate on the metallic regime where conductivity $\sigma \gg e^2/h$. We have found that in this system subjected to parallel magnetic fields, the spin susceptibility of band electrons (Pauli spin susceptibility) becomes enhanced by almost an order of magnitude at low electron densities, growing critically near a certain critical density $n_\chi \approx 8 \times 10^{10} \text{ cm}^{-2}$: behavior that is characteristic in the close vicinity of a phase transition. The density n_χ is coincident within the experimental uncertainty with the critical density n_c for the zero-field metal-insulator transition (MIT) in our samples. We have also found by measurements in perpendicular and tilted magnetic fields that the g -factor is weakly enhanced and practically independent of the electron density down to the lowest densities reached, while the cyclotron mass becomes strongly enhanced at low n_s . Thus, unlike in the Stoner scenario, it is the effective mass, rather than the g -factor, that is responsible for the dramatically enhanced spin susceptibility at low electron densities.

2 Experimental setup and samples

Magnetization is one of the least studied properties of 2D electron systems: signals associated with it are weak making measuring them a challenging ex-

periment. Few experimental observations of the de Haas-van Alphen effect in 2D electron systems were made using SQUID magnetometers [8], pick up coils lithographed above the gate [9], or torque magnetometers [10]. Here we use a novel method [11] to measure the magnetization that entails modulating the magnetic field with an auxiliary coil and measuring the AC current induced between the gate and the 2D electron system. The experimental set-up is shown in Fig. 1 (a). Magnetic field B was modulated with a small ac field δB in the range $0.005 - 0.03$ T at frequencies between $f = 0.05$ and 0.45 Hz. The in-phase and out-of-phase components of the current between the gate and the 2D electron system were measured with high precision ($\sim 10^{-16}$ A) using a current-voltage converter and a lock-in amplifier. The real (in-phase) component of the current depends on the dissipative conductivity σ of the sample. We are, however, interested in the imaginary (out-of-phase) current

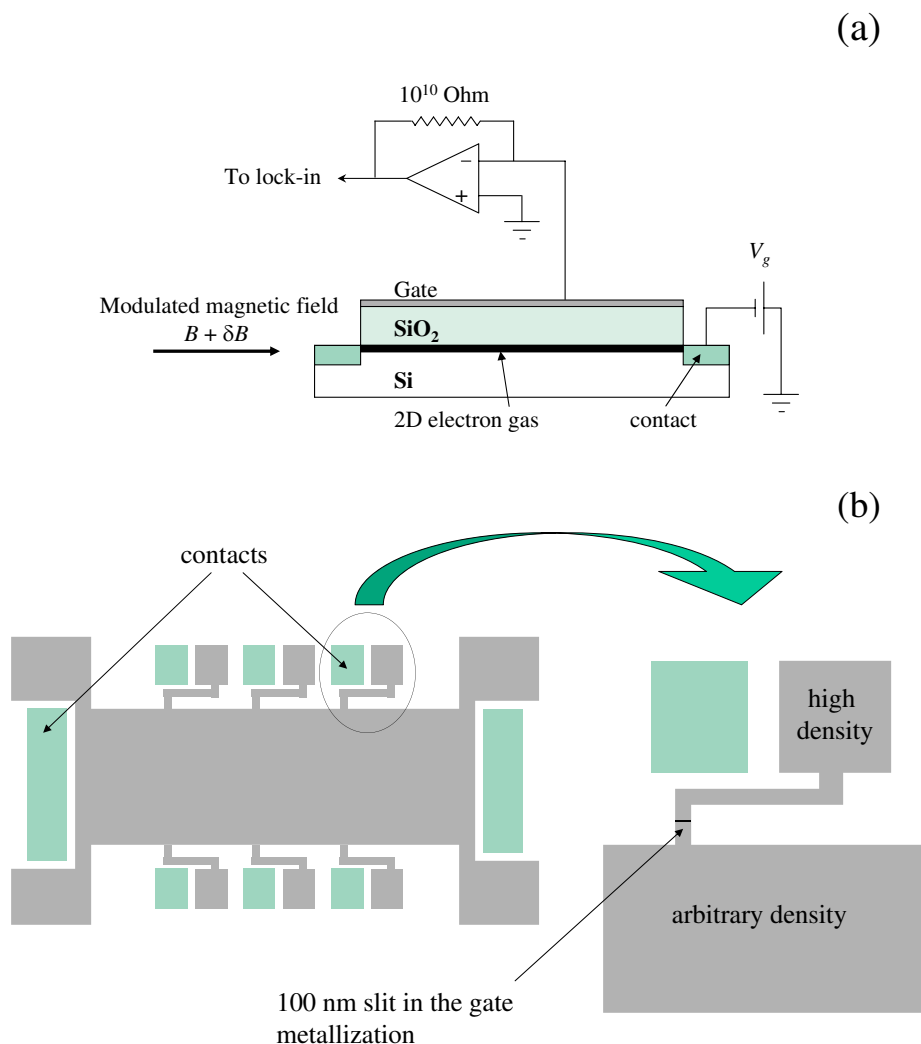


Fig. 1. (a) Experimental set-up for measurements of thermodynamic magnetization. (b) Top view of a MOSFET with slit in the gate metalization indicated.

component, which, under condition that $2\pi fC \ll \sigma$, is equal to

$$\text{Im } i = \frac{2\pi fC}{e} \frac{d\mu}{dB} \delta B, \quad (1)$$

where C is the capacitance of the sample measured in the same experiment and μ is the chemical potential. Use of ultra-low frequencies ensures that $2\pi fC \ll \sigma$ and the out-of-phase current component is not contaminated by lateral transport effects. By applying the Maxwell relation $dM/dn_s = -d\mu/dB$, one can then obtain the magnetization M from the measured i . For measurements of the thermodynamic density of states, a similar circuit was used with a distinction that the gate voltage was modulated and thus the imaginary current component was proportional to the capacitance. Thermodynamic density of states $dn_s/d\mu$ is related to magnetocapacitance via

$$\frac{1}{C} = \frac{1}{C_0} + \frac{1}{Ae^2(dn_s/d\mu)}, \quad (2)$$

where C_0 is the geometric capacitance and A is the sample area.

Measurements were made in an Oxford dilution refrigerator on low-disordered (100)-silicon metal-oxide-semiconductor field-effect transistors (MOSFETs). These samples are remarkable by the absence of a band tail of localized electrons down to electron densities $n_s \approx 1 \times 10^{11} \text{ cm}^{-2}$ [6], which allows one to study properties of a *clean* 2D electron system without admixture of local moments [12,13,14]. The level of disorder is determined by the quality of the Si-SiO₂ interface. The silicon oxide layer in our samples was grown repeatedly during several stages of the fabrication to decrease number of charged impurities and obtain high quality interface; as a result, in samples with oxide thickness of 149 nm, we have achieved peak mobilities of 3 m²/Vs at $T = 100$ mK. The second advantage of these samples is a very low contact resistance (in “conventional” silicon samples, high contact resistance becomes the main experimental obstacle in the low density/low temperature limit). To minimize contact resistance, thin slits in the gate metalization have been introduced (see Fig. 1 (b)), which allows for maintaining high electron density near the contacts regardless of its value in the main part of the sample.

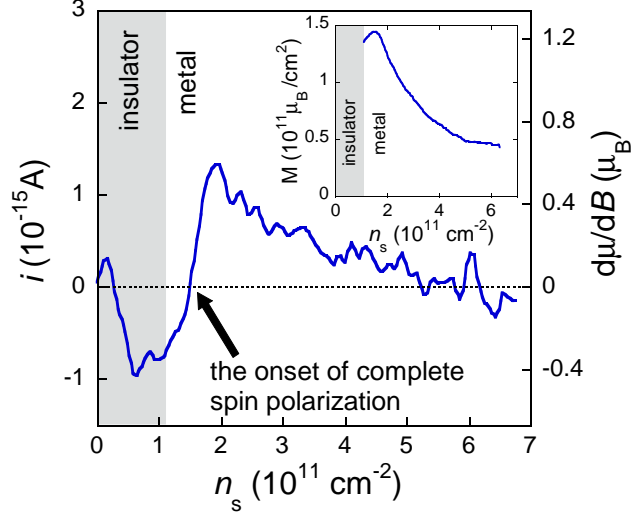


Fig. 2. Imaginary current component in the magnetization experiment as a function of the electron density in a magnetic field of 5 T and $T = 0.4$ K. Grey area depicts the insulating phase. Magnetization versus n_s is displayed in the inset. Note that the maximum M is coincident within the experimental uncertainty with $\mu_B n_s$.

3 Experimental results and discussion

3.1 Pauli spin susceptibility

We start with measurements of Pauli spin susceptibility. A typical experimental trace of $i(n_s)$ in a parallel magnetic field of 5 T is displayed in Fig. 2. The inset shows magnetization $M(n_s)$ in the metallic phase obtained by integrating $dM/dn_s = -d\mu/dB$ with the integration constant $M(\infty) = B\chi_0$, where χ_0 is the Pauli spin susceptibility of non-interacting electrons. A nearly anti-symmetric jump of $i(n_s)$ about zero on the y -axis (marked by the black arrow) separates the high- and low-density regions in which the signal is positive and negative ($M(n_s)$ is decreasing and increasing), respectively. Such a behavior is expected based on simple considerations. At low densities, all electrons are spin-polarized in a magnetic field, so for the simple case of non-interacting 2D electrons one expects $d\mu/dB = -\mu_B$ (at $n_s \rightarrow 0$, deep in the insulating regime, the capacitance of the system vanishes and, therefore, the measured current approaches zero). At higher densities, when the electrons start to fill the upper spin subband, $M(n_s)$ starts to decrease, and $d\mu/dB$ is determined by the renormalized Pauli spin susceptibility χ and is expected to decrease with n_s due to reduction in the strength of electron-electron interactions. Finally, in the high-density limit, the spin susceptibility approaches its “non-interacting” value χ_0 , and $d\mu/dB$ should approach zero. The onset of complete spin polarization — the electron density n_p at which the electrons start to fill the upper spin subband — is given by the condition $d\mu/dB = 0$

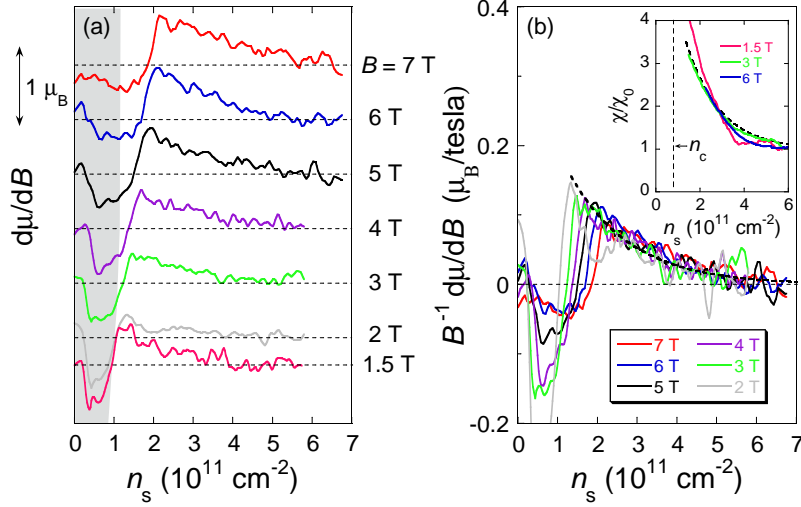


Fig. 3. (a) The experimental $d\mu/dB$ as a function of electron density in different magnetic fields and $T = 0.4$ K. The curves are vertically shifted for clarity. Grey area depicts the insulating phase. Note that the onset of full spin polarization in our experiment always takes place in the metallic regime. (b) Scaling of the $d\mu/dB$ curves, normalized by magnetic field magnitude, at high electron densities. The dashed line represents the “master curve”. Spin susceptibility obtained by integrating the master curve (dashed line) and raw data at $B = 1.5, 3$, and 6 T is displayed in the inset.

($M(n_s)$ reaches a maximum), as indicated by the black arrow in the figure. It is important that over the range of magnetic fields used in the experiment (1.5–7 tesla), the maximum M coincides within the experimental uncertainty with $\mu_B n_s$ thus confirming that all the electrons are indeed spin-polarized below n_p . Note however that the absolute value of $d\mu/dB$ at $n_s \lesssim n_c$ is reduced in the experiment. We attribute this to smearing of the minimum in $i(n_s)$ caused by possible influence of the residual disorder in the electron system, which is crucial in and just above the insulating phase, in contrast to the clean metallic regime we focus on here. Another reason for the reduction in $d\mu/dB$ is the electron-electron interactions (due to, *e.g.*, the enhanced effective mass).

In Fig. 3(a), we show a set of curves for the experimental $d\mu/dB$ versus electron density in different magnetic fields. Experimental results in the range of magnetic fields studied do not depend, within the experimental noise, on temperature below 0.6 K (down to 0.15 K which was the lowest temperature achieved in this experiment). The onset of full spin polarization shifts to higher electron densities with increasing magnetic field. Grey area depicts the insulating phase, which expands somewhat with B (for more on this, see Ref. [15]). Note that the range of magnetic fields used in our experiment is restricted from below by the condition that $d\mu/dB$ crosses zero in the metallic regime. In Fig. 3(b), we show how these curves, normalized by magnetic field, collapse in the partially-polarized regime onto a single “master curve”. The existence of such scaling verifies proportionality of the magnetization to B ,

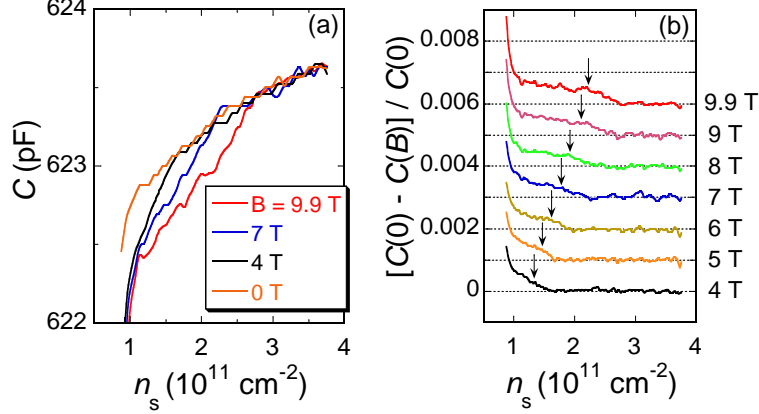


Fig. 4. (a) Magnetocapacitance versus electron density for different magnetic fields. (b) Deviation of the $C(n_s)$ dependences for different magnetic fields from the $B = 0$ reference curve. The traces are vertically shifted for clarity. The onset of full spin polarization is indicated by arrows.

confirming that we deal with Pauli spin susceptibility of band electrons, and establishes a common zero level for the experimental traces. Integration of the master curve over n_s yields the spin susceptibility $\chi = M/B$, as shown in the inset to Fig. 3(b). Also shown is the spin susceptibility obtained by integration of raw curves at $B = 1.5, 3$, and 6 tesla, which, within the experimental error, yield the same dependence.

This method of measuring the spin susceptibility, being the most direct, suffers, however, from possible influence of the unknown diamagnetic contribution to the measured $d\mu/dB$, which arises from the finite width of the 2D electron layer [16]. To verify that this influence is negligible in our samples, we employ another two independent methods to determine χ . The second method is based on marking the electron density n_p at which $d\mu/dB = 0$ and which corresponds to the onset of complete spin polarization, as mentioned above. The so-determined polarization density $n_p(B)$ can be easily converted into $\chi(n_s)$ via $\chi = \mu_B n_p / B$. Note that in contrast to the value of $d\mu/dB$, the polarization density n_p is practically not affected by possible influence of the diamagnetic shift.

The third method for measuring n_p and χ , insensitive to the diamagnetic shift, relies on analyzing the magnetocapacitance, C . Experimental traces $C(n_s)$ are shown in Fig. 4(a) for different magnetic fields. As the magnetic field is increased, a step-like feature emerges on the $C(n_s)$ curves and shifts to higher electron densities. This feature corresponds to the thermodynamic density of states abruptly changing when the electrons' spins become completely polarized. To see the step-like feature more clearly, in Fig. 4(b) we subtract the $C(n_s)$ curves for different magnetic fields from the reference $B = 0$ curve. The fact that the jumps in C (as well as in $d\mu/dB$) are washed out much stronger than it can be expected from possible inhomogeneities in the electron density

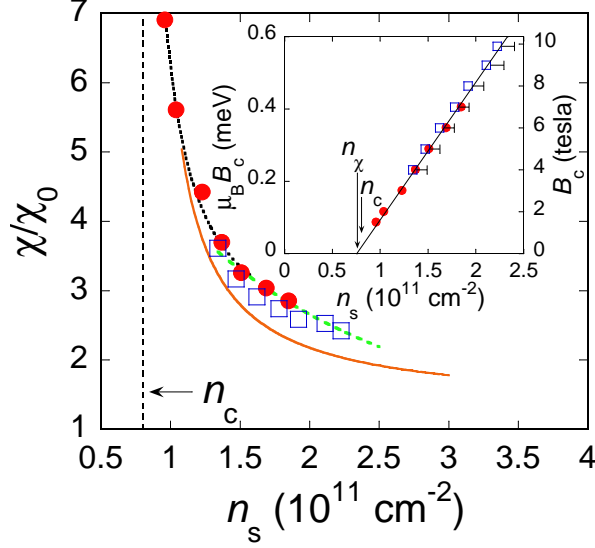


Fig. 5. Dependence of the Pauli spin susceptibility on electron density obtained by all three methods described in text: integral of the master curve (dashed line), $d\mu/dB = 0$ (circles), and magnetocapacitance (squares). The dotted line is a guide to the eye. Also shown by a solid line is the transport data of Ref. [7]. Inset: polarization field as a function of the electron density determined from the magnetization (circles) and magnetocapacitance (squares) data. The symbol size for the magnetization data reflects the experimental uncertainty, and the error bars for the magnetocapacitance data extend to the middle of the jump in C . The data for B_c are described by a linear fit which extrapolates to a density n_χ close to the critical density n_c for the $B = 0$ MIT.

distribution (about $4 \times 10^9 \text{ cm}^{-2}$ [7]) points to the importance of electron-electron interactions. Since the effects of interactions are different in the fully- and partially-polarized regimes, it is natural to mark the onset of full spin polarization at the beginning of the interaction-broadened jump, as indicated by arrows in the figure. In case the residual disorder does contribute to the jump broadening, we extend error bars to the middle of the jump, which yields an upper boundary for the onset of full spin polarization.

In Fig. 5, we show the summary of the results for the Pauli spin susceptibility as a function of n_s , obtained using all three methods described above. The excellent agreement between the results obtained by all of the methods establishes that a possible influence of the diamagnetic shift is negligible [17] and, therefore, the validity of the data including those at the lowest electron densities is justified. There is also good agreement between these results and the data obtained by the transport experiments of Ref. [7]. This adds credibility to the transport data and confirms that full spin polarization occurs at the field B_c ; however, we note again that evidence for the phase transition can only be obtained from thermodynamic measurements. The magnetization data extend to lower densities than the transport data, and larger values of χ are reached, exceeding the “non-interacting” value χ_0 by almost an order of

magnitude. The Pauli spin susceptibility behaves critically close to the critical density n_c for the $B = 0$ metal-insulator transition [18]: $\chi \propto n_s/(n_s - n_\chi)$. This is in favor of the occurrence of a spontaneous spin polarization (either Wigner crystal [19] or ferromagnetic liquid) at low n_s , although in currently available samples, the formation of the band tail of localized electrons at $n_s \lesssim n_c$ conceals the origin of the low-density phase. In other words, so far, one can only reach an incipient transition to a new phase.

The dependence $B_c(n_s)$, determined from the magnetization and magnetocapacitance data, is represented in the inset to Fig. 5. The two data sets coincide and are described well by a common linear fit which extrapolates to a density n_χ close to n_c . We emphasize that in the low-field limit ($B < 1.5$ tesla), the jump in $d\mu/dB$ shifts to the insulating regime, which does not allow us to approach closer vicinity of n_χ : based on the data obtained in the regime of strong localization, one would not be able to make conclusions concerning properties of a clean metallic electron system which we are interested in here. Clearly, the fact that the linear $B_c(n_s)$ dependence persists down to the lowest electron densities achieved in the experiment confirms that we always deal with the clean metallic regime.

In the end of this subsection, we would like to clarify the principal difference between our results and those of Ref. [11]. In the sample used by Prus *et al.*, the critical density n_c for the $B = 0$ MIT was considerably higher than in our samples caused by high level of disorder, and the band tail of localized electrons was present at all electron densities [11]. As a result, the crucial region of low electron densities, in which the critical behavior of the Pauli spin susceptibility occurs, falls within the insulating regime where the physics of local moments dominates [12,13,14]. Indeed, Prus *et al.* have found sub-linear $M(B)$ dependence characteristic of local moments, and the extracted spin susceptibility in their sample has a Curie temperature dependence [14]. This is the case even at high electron densities, where metallic behavior might be expected instead. Such effects are absent in our samples: the spin susceptibility (in the partially-polarized system) is independent of the magnetic field and temperature, confirming that we deal with Pauli spin susceptibility of band electrons.

3.2 Magnetization in perpendicular magnetic fields: g -factor and effective mass

Typical experimental traces of the gate current in a perpendicular magnetic field of 5 T are displayed in Fig. 6. Sharp dips in the out-of-phase component, seen at integer filling factors $\nu \equiv n_s hc/eB_\perp$, reflect gaps in the density of states: dips at odd filling factors correspond to the valley splitting, the ones

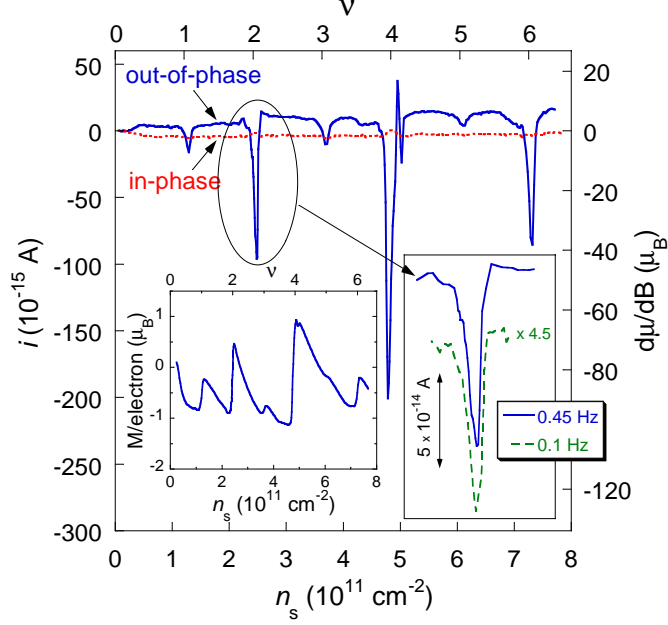


Fig. 6. Out-of-phase (solid line) and in-phase (dotted line) current components as a function of the electron density in a perpendicular magnetic field of 5 T and $T = 0.8$ K. $\delta B = 0.022$ T and $f = 0.45$ Hz. The value $d\mu/dB$ is indicated in units of the Bohr magneton μ_B . In the right-hand inset, we demonstrate proportionality of $\text{Im } i$ to frequency: the solid and dashed lines (vertically shifted for clarity) correspond to 0.45 and 0.1 Hz, respectively; the y -component of the latter is multiplied by 4.5. The left-hand inset illustrates magnetization per electron.

at $\nu = 2$ and 6 are due to the spin splitting, and the dip at $\nu = 4$ is due to the cyclotron splitting. However, there are no corresponding features in the in-phase current component, which ensures that we reach the low-frequency limit and the measured $\partial\mu/\partial B$ is not distorted by lateral transport effects. This is further confirmed by the fact that the out-of-phase current is proportional to the excitation frequency as displayed in the right-hand inset to Fig. 6. Magnetization per electron can be extracted by integrating the measured out-of-phase signal with respect to n_s , as shown in the left-hand inset to Fig. 6 for illustration. The magnetization exhibits the expected sawtooth oscillations, with sharp jumps at integer filling factors (note that the height of the jumps yields values that are smaller than the level splitting by the level width).

If the disorder and interactions are disregarded, in quantizing magnetic fields (except at integer filling factors) the derivative $\partial\mu/\partial B = -\partial M/\partial n_s$ is equal to

$$\frac{\partial\mu}{\partial B} = \mu_B \left[\left(\frac{1}{2} + N \right) \frac{2m_e}{m_b} \pm \frac{1}{2}g_0 \right], \quad (3)$$

where μ_B is the Bohr magneton, N is the Landau level number, m_e and $m_b = 0.19 m_e$ are the free electron mass and band mass, respectively, and

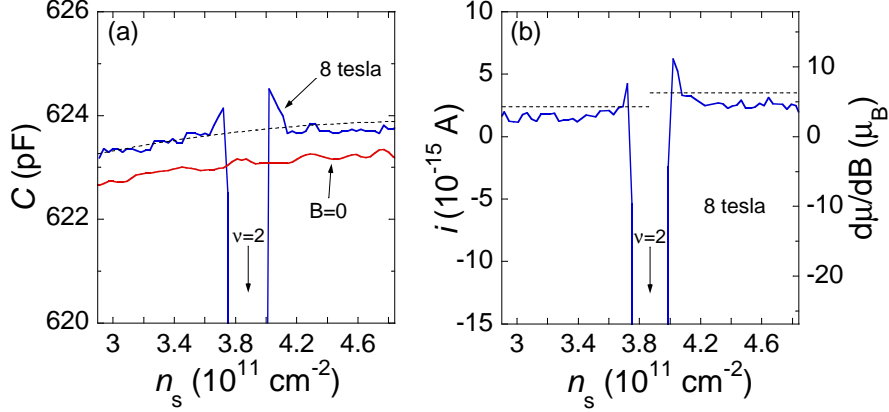


Fig. 7. (a) Capacitance in $B = 8$ tesla and in $B = 0$ as indicated. The (noise averaged) geometric capacitance is depicted by a dashed line. (b) $\text{Im } i \propto d\mu/dB$ in a perpendicular magnetic field of 8 tesla. The maximum values possible in a non-interacting system (see text) are depicted by dashed lines.

$g_0 = 2$ is the g -factor in bulk silicon. Disorder smears out the dependences which otherwise would consist of a series of delta-functions. Interactions modify this picture in two ways: (i) by renormalizing the values of the cyclotron mass and g -factor and (ii) by providing a negative contribution of order $-(e^2/\epsilon l_B)\{\nu\}^{1/2}$ to the chemical potential [21,22] (here ϵ is the dielectric constant, l_B is the magnetic length, and $\{\nu\}$ is the deviation of the filling factor from the nearest integer). The latter effect, which is caused by the intra-level interactions between quasiparticles, leads to the so-called negative thermodynamic compressibility near integer filling factors predicted by Efros [22] and experimentally observed in Refs. [23,24].

In Fig. 7, we compare capacitance C with $\partial\mu/\partial B$, measured at the same magnetic field value and plotted versus n_s around the filling factor $\nu = 2$. The geometric capacitance [25] (the inverse of the first term in Eq. (2)), depicted by dashed line in Fig. 7(a), slightly increases with n_s since the thickness of the 2D electron layer — and, therefore, the average distance between the 2D layer and the gate — decreases with the gate voltage. The second term in Eq. (2) is responsible for the dip centered at $n_s = 3.87 \times 10^{11} \text{ cm}^{-2}$, corresponding to $\nu = 2$, and sharp maxima on both sides of it. Note that at these maxima, the capacitance exceeds C_0 , which corresponds to the negative thermodynamic compressibility discussed above. Farther from integer filling factors, the intra-level interaction corrections become weak, being proportional to $\{\nu\}^{-1/2}$, and the measured capacitance approaches C_0 (as long as the broadening of Landau levels is negligible, *i.e.*, $dn_s/d\mu \gg dn_s/d\mu|_{B=0}$).

Similar maxima on both sides of $\nu = 2$ are seen in the magnetization data shown in Fig. 7 (b). At the maxima, the derivative $\partial\mu/\partial B$ exceeds maximum values possible in a non-interacting 2D electron gas, which are determined by Eq. (3) and are depicted in the figure by dashed lines. The possibility that

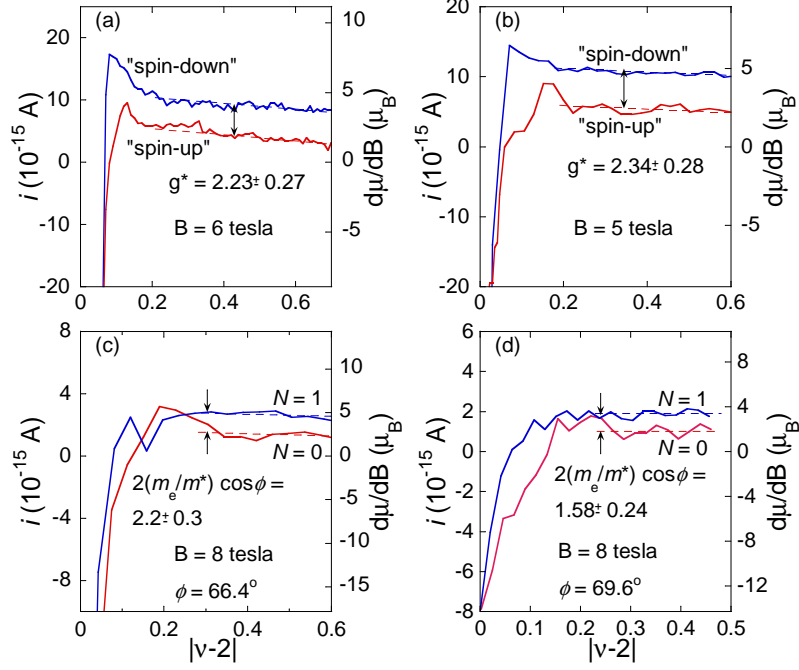


Fig. 8. Illustration of how the effective g -factor (a, b) and the cyclotron mass (c, d) have been measured. The imaginary current component is plotted as a function of the deviation of the filling factor from $\nu = 2$. In perpendicular magnetic fields, the difference between $\partial\mu/\partial B$ for spin-down (\downarrow) and spin-up (\uparrow) electrons yields g^* in units of the Bohr magneton. In tilted magnetic fields, the difference between $\partial\mu/\partial B$ for electrons with $N = 1$ and $N = 0$ is equal to $2\mu_B (m_e/m^*) \cos \phi$. The dashed lines show noise-averaged values. $\delta B = 0.022$ T (a, b) and 0.0055 T (c, d).

$\partial\mu/\partial B$ might exceed its maximum non-interacting values due to intra-level Coulomb interactions between quasiparticles was predicted by MacDonald *et al.* [21]; in fact, this is how negative compressibility [22] manifests itself in magnetization measurements. Sharp spike just above $\nu = 4$ and maxima on both sides of $\nu = 2$ in the dependence shown in Fig. 6 are of the same nature.

It is straightforward to obtain the effective g -factor from the data for $\partial\mu/\partial B$. In accordance with Eq. (3), it is equal (in units of the Bohr magneton) to the difference between $\partial\mu/\partial B$ for spin-down (\downarrow) and spin-up (\uparrow) electrons belonging to the same Landau level: $\mu_B g^* = (\partial\mu/\partial B)_\downarrow - (\partial\mu/\partial B)_\uparrow$. It is important that this method of determining the g -factor does not require the use of any fitting procedures or parameters. Figure 8 (a, b) shows measured $\partial\mu/\partial B$ as a function of the deviation of the filling factor from 2 at two values of magnetic field. Near $\nu = 2$, there are sharp intra-level interaction-induced structures discussed above; these regions have been excluded from the analysis. However, farther from $\nu = 2$, the dependences for $\nu < 2$ and $\nu > 2$ become parallel to each other. This ensures that the so-determined g^* is not affected by the valley splitting [26,27] and intra-level interaction effects [21,22] discussed above. The latter contribute equally to both spin-up and spin-down dependences and can-

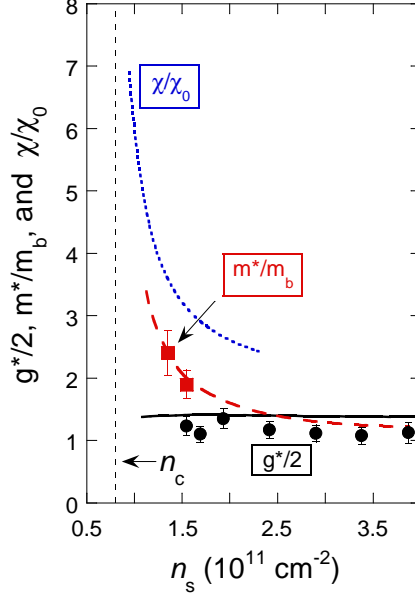


Fig. 9. The effective g -factor (circles) and the cyclotron mass (squares) as a function of the electron density. The solid and long-dashed lines represent, respectively, the g -factor and effective mass, previously obtained from transport measurements [28], and the dotted line is the Pauli spin susceptibility obtained by magnetization measurements in parallel magnetic fields. The critical density n_c for the $B = 0$ metal-insulator transition is indicated.

cel each other out. Disorder also contributes equally to $\partial\mu/\partial B$ on both sides of $\nu = 2$: we have found that at magnetic fields down to approximately 3 T, there are wide regions of filling factors where capacitance (*i.e.*, the density of states) is symmetric around $\nu = 2$ (see, *e.g.*, Fig. 7 (a)); furthermore, closeness of the capacitance to C_0 attests that the disorder-induced corrections are small. At lower magnetic fields, however, the electron-hole symmetry around $\nu = 2$ breaks down, which sets the lower boundary for the range of magnetic fields (and, consequently, electron densities). Note that temperature smears out the dependences in a way similar to disorder: at higher temperatures, the capacitance at half-integer filling factors decreases, which leads to a worsening of the method accuracy.

In Fig. 9 we plot the measured g -factor along with the one previously obtained from transport measurements (solid line). One can see that there is no systematic dependence of the g -factor on n_s : it remains approximately constant and close to its value in bulk silicon even at the lowest electron densities, which is in good agreement with the transport [28] and magnetocapacitance [26] results.

The same method can be used for determination of the cyclotron mass in tilted magnetic fields strong enough to completely polarize the electron spins [29]. If (and only if) the spin splitting exceeds the cyclotron splitting, the gap at $\nu = 2$ lies between Landau levels $0\uparrow$ and $1\uparrow$, and the difference $(\partial\mu/\partial B)_{N=1} -$

$(\partial\mu/\partial B)_{N=0}$ is equal to $2\mu_B (m_e/m^*) \cos \phi$, where ϕ is the tilt angle. Once the electron spins are fully polarized at filling factors above $\nu = 2$, the tilt angle is automatically large enough for the level crossing to have occurred. The region of explorable electron densities is restricted from above by the condition that the electrons must be fully spin-polarized, while with our current set-up, the maximum magnetic field at which we can apply the modulation is only 8 tesla capable of polarizing the electron spins up to $n_s^* \approx 2 \times 10^{11} \text{ cm}^{-2}$ (see previous subsection and Ref. [30]). Figure 8 (c, d) shows $\partial\mu/\partial B$ as a function of $|\nu - 2|$ under the condition $n_s < n_s^*$ at two tilt angles [31]. The extracted cyclotron mass at electron densities 1.55 and $1.35 \times 10^{11} \text{ cm}^{-2}$ is significantly enhanced. At densities below $1.35 \times 10^{11} \text{ cm}^{-2}$, the symmetry of capacitance on both sides of the $\nu = 2$ gap breaks down, making the determination of m^* impossible. As a result, we were only able to obtain two data points. Nevertheless, good agreement with the effective mass previously obtained by transport measurements (Fig. 9) demonstrates the applicability of the new method and adds credibility to both transport and magnetization results.

We stress once again that the advantage of the new method we use here is that it allows determination of the spectrum of the 2D electron system under the condition that the Fermi level lies outside the spectral gaps, and the inter-level interactions are avoided. Being symmetric about $\nu = 2$, the intra-level interactions are canceled out in the data analysis and do not influence the extracted g -factor and cyclotron mass. Therefore, the obtained values g^* and m^* are likely to be identical with those for a continuous spectrum, and the comparison with previously found values of the g -factor and the effective mass is valid.

4 Conclusions

The Pauli spin susceptibility has been determined by measurements of the thermodynamic magnetization and density of states in a low-disordered, strongly correlated 2D electron system in silicon in parallel magnetic fields. It is found to behave critically near the zero-field MIT, which is characteristic of the existence of a phase transition. Magnetization measurements in perpendicular and tilted magnetic fields allow determination of the spectrum characteristics of 2D electron systems and show that enhancement of the g -factor is weak and practically independent of the electron density, while the cyclotron mass becomes strongly enhanced as the density is decreased. The obtained data agree well with the g -factor and effective mass obtained by transport measurements, as well as with the Pauli spin susceptibility obtained by magnetization measurements in parallel magnetic fields, even though the lowest electron densities reached in the second experiment are somewhat higher. Thus, we arrive at the conclusion that, unlike in the Stoner scenario, it is indeed the effective

mass that is responsible for the dramatically enhanced spin susceptibility at low electron densities. This result is consistent with conclusions of the recent theory by Punnoose and Finkelstein [32] who made a renormalization group analysis for multi-valley 2D systems and found that the effective mass dramatically increases at the metal-insulator transition while the g -factor remains nearly intact. We note, however, that the theoretical spin susceptibility diverges at disorder-dependent density n_c [32], whereas the experimental χ grows critically near the disorder-independent density n_χ [6].

Acknowledgments

We gratefully acknowledge discussions with S. Chakravarty, B. I. Halperin, D. Heiman, N. E. Israeloff, R. S. Markiewicz, and M. P. Sarachik. We would also like to thank A. Gaidarzhy and J. B. Miller for technical assistance and C. M. Marcus and P. Mohanty for an opportunity to use their nanofabrication facilities. This work was supported by NSF grant DMR-0403026, PRF grant 41867-AC10, the RFBR, RAS, and the Programme “The State Support of Leading Scientific Schools”.

References

- [1] L. D. Landau, Sov. Phys. JETP **3**, 920 (1957).
- [2] E. Wigner, Phys. Rev. **46**, 1002 (1934).
- [3] B. Tanatar and D. M. Ceperley, Phys. Rev. B **39**, 5005 (1989); G. Benenti, X. Waintal, and J.-L. Pichard, Phys. Rev. Lett. **83**, 1826 (1999); C. Attacalite, S. Moroni, P. Gori-Giorgi, and G. B. Bachelet, Phys. Rev. Lett. **88**, 256601 (2002).
- [4] H. von Löhneysen, Advances in Solid State Physics **30**, 95 (1990).
- [5] T. Okamoto, K. Hosoya, S. Kawaji, and A. Yagi, Phys. Rev. Lett. **82**, 3875 (1999); J. Zhu, H. L. Stormer, L. N. Pfeiffer, K. W. Baldwin, and K. W. West, Phys. Rev. Lett. **90**, 056805 (2003).
- [6] S. V. Kravchenko and M. P. Sarachik, Rep. Prog. Phys. **67**, 1 (2004); A. A. Shashkin, Phys. Usp. **48**, 129 (2005).
- [7] A. A. Shashkin, S. V. Kravchenko, V. T. Dolgoplov, and T. M. Klapwijk, Phys. Rev. Lett. **87**, 086801 (2001).
- [8] H. Stormer, T. Haavasoja, V. Narayanamurti, A. C. Gossard, and W. Wiegmann, J. Vac. Sci. Tech. B **1**, 423 (1983); I. Meinel, D. Grundler, S.

- Bargstadt-Franke, C. Heyn, and D. Heitmann, Appl. Phys. Lett. **70**, 3305 (1997).
- [9] F. F. Fang and P. J. Stiles, Phys. Rev. B **28**, 6992 (1983).
- [10] J. P. Eisenstein, Appl. Phys. Lett. **46**, 695 (1985); J. P. Eisenstein, H. L. Stormer, V. Narayanamurti, A. Y. Cho, A. C. Gossard, and C. W. Tu, Phys. Rev. Lett. **55**, 875 (1985); S. A. J. Wieggers, M. Specht, L. P. Levy, M. Y. Simmons, D. A. Ritchie, A. Cavanna, B. Etienne, G. Martinez, and P. Wyder, Phys. Rev. Lett. **79**, 3238 (1997); M. Zhu, A. Usher, A. J. Matthews, A. Potts, M. Elliott, W. G. Herrenden-Harker, D. A. Ritchie, and M. Y. Simmons, Phys. Rev. B **67**, 155329 (2003).
- [11] O. Prus, Y. Yaish, M. Reznikov, U. Sivan, and V. Pudalov, Phys. Rev. B **67**, 205407 (2003).
- [12] N. F. Mott and E. A. Davis, *Electronic Processes in Non-Crystalline Materials* (Clarendon Press, Oxford, United Kingdom, 1971).
- [13] V. T. Dolgoplov and A. Gold, Phys. Rev. Lett. **89**, 129701 (2002).
- [14] A. Gold and V. T. Dolgoplov, J. Phys.: Condens. Matter **14**, 7091 (2002).
- [15] A. A. Shashkin, S. V. Kravchenko, and T. M. Klapwijk, Phys. Rev. Lett. **87**, 266402 (2001).
- [16] To deal with this problem, the “subtraction of the diamagnetic contribution” was suggested in Ref. [11]. The diamagnetic contribution Δ was determined in the partially-polarized regime as the difference between the direct magnetization data (“Mag”) and the data obtained from Shubnikov-de Haas oscillations (“SdH”): $\Delta = \text{Mag} - \text{SdH}$. The experimental data were then corrected by Δ . We find this procedure meaningless as it essentially results in replacing the magnetization data by Shubnikov-de Haas data: $\text{Mag} - \Delta = \text{Mag} - (\text{Mag} - \text{SdH}) = \text{SdH}$. In fact, the difference between magnetization and Shubnikov-de Haas data in their experiment is likely to be due to the presence of a band tail of localized electrons at all electron densities in their sample.
- [17] Since the diamagnetic shift decreases with increasing n_s and/or decreasing B , it may in principle be noticeable at the lowest n_s and highest B used in the experiment. Comparing low- and high-field curves shown in Fig. 3(a), we estimate that at $n_s \sim 1 \times 10^{11} \text{ cm}^{-2}$ and $B = 7 \text{ T}$, the contribution of the diamagnetic shift is less than $0.2\mu_B$.
- [18] The critical density for the MIT was determined from transport measurements (see Refs. [6,15]).
- [19] The fact that $B_c \rightarrow 0$ as $n_s \rightarrow n_c$ speaks in favor of the strongly correlated liquid being close to the crystal [20].
- [20] B. Castaing and P. Nozières, J. Phys. (Paris) **40**, 257 (1979).
- [21] A. H. MacDonald, H. C. A. Oji, and K. L. Liu, Phys. Rev. B **34**, 2681 (1986).

- [22] A. L. Efros, Solid State Commun. **65**, 1281 (1988).
- [23] S. V. Kravchenko, V. M. Pudalov, and S. G. Semenchinsky, Phys. Lett. A **141**, 71 (1989).
- [24] J. P. Eisenstein, L. N. Pfeiffer, and K. W. West, Phys. Rev. Lett. **68**, 674 (1992).
- [25] The geometric capacitance has been determined according to $1/C_0 = 1/C|_{B=0} - 1/Ae^2 (dn_s/d\mu)|_{B=0}$ (for more on this procedure, see Ref. [26]).
- [26] V. S. Khrapai, A. A. Shashkin, and V. T. Dolgoplov, Phys. Rev. Lett. **91**, 126404 (2003); Phys. Rev. B **67**, 113305 (2003).
- [27] The bare valley splitting is independent of the magnetic field and does not contribute to $\partial\mu/\partial B$. However, it may be enhanced by inter-level interactions [26]. The fact that $\partial\mu/\partial B$ for $\nu < 2$ and $\nu > 2$ are parallel to each other ensures that a possible influence of the enhanced valley splitting is negligible in our experiment.
- [28] A. A. Shashkin, S. V. Kravchenko, V. T. Dolgoplov, and T. M. Klapwijk, Phys. Rev. B **66**, 073303 (2002).
- [29] The effects of finite layer thickness, which lead to an increase of the effective mass with parallel magnetic field, are negligible in silicon MOSFETs [6].
- [30] S. A. Vitkalov, H. Zheng, K. M. Mertes, M. P. Sarachik, and T. M. Klapwijk, Phys. Rev. Lett. **85**, 2164 (2000).
- [31] Using $n_s^*(8 \text{ T}) \approx 2 \times 10^{11} \text{ cm}^{-2}$, one can estimate that the coincidence of spin and cyclotron splittings for $\nu = 2$ occurs at $\phi^* = \cos^{-1}(n_s^*hc/2eB) \approx 59^\circ$.
- [32] A. Punnoose and A. M. Finkelstein, Science **310**, 289 (2005).